The Astrophysical Journal, 870:59 (10pp), 2019 January 10 https://doi.org/10.3847/1538-4357/aaf1a3

ALMA, ATCA, and *Spitzer* Observations of the Luminous Extragalactic Supernova SN 1978K

I. A. Smith[1], S. D. Ryder[2,3], R. Kotak[4], E. C. Kool[2,3], and S. K. Randall[5]
[1] Department of Physics and Astronomy, Rice University, 6100 South Main, MS-108, Houston, TX 77251-1892, USA; iansmith@rice.edu
[2] Australian Astronomical Observatory, 105 Delhi Road, North Ryde, NSW 2113, Australia
[3] Department of Physics and Astronomy, Macquarie University, NSW 2109, Australia
[4] Department of Physics and Astronomy, University of Turku, Vesilinnantie 5, FI-20014, Finland
[5] European Southern Observatory, Karl-Schwarzschild-Straße 2, D-85748, Garching, Germany
Received 2018 July 26; revised 2018 November 6; accepted 2018 November 14; published 2019 January 8

Abstract

Only three extragalactic supernovae have been detected at late times at millimeter wavelengths: SN 1987A, SN 1978K, and SN 1996cr. SN 1978K is a remarkably luminous Type IIn supernova that remains bright at all wavelengths 40 years after its explosion. Here, we present Atacama Large Millimeter/submillimeter Array (ALMA) observations taken in 2016 using Bands 3, 4, 6, and 7 that show a steepening in the spectrum. An absorbed single power-law model broadly fits all of the radio and millimeter observations, but would require significant chromatic variability. Alternatively, a broken power law fits the radio-millimeter spectrum; this can be explained using an ultra-relativistic spherical blast wave in a wind scaling with a cooling break, as in a gamma-ray burst afterglow. Using updated Australia Telescope Compact Array light curves, we show that the non-thermal radio continuum continues to decay as $t^{-1.53}$; in the fireball model, this independently defines the power-law indices found in the radio-millimeter spectrum. Supernovae such as SN 1978K might be important contributors to the universal dust budget: only SN 1978K was detected in a search for warm dust in supernovae in the transitional phase (age 10–100 yr). Using *Spitzer Space Telescope* observations, we show that at least some of this dust emission has been decaying rapidly as $t^{-2.45}$ over the past decade, suggesting it is being destroyed. Depending on the modeling of the synchrotron emission, the ALMA observations suggest there may be emission from a cold dust component.

Key words: galaxies: individual (NGC 1313) – gamma-ray burst: general – supernovae: general – supernovae: individual (SN 1978K)

1. Introduction

SN 1978K was only the second supernova to be detected and recognized as a supernova from its radio emission and the first from its X-rays (Ryder et al. 1993). Although the date of the explosion (t_0) remains unknown, we assume it was 1978 May 22 (MJD 43650), as adopted by Montes et al. (1997). It is rare that supernovae are bright enough to be followed in the X-ray band (Bregman et al. 2003), and SN 1978K is one of only a few that have had long-term multi-wavelength monitoring; it remains bright at all wavelengths 40 years after the explosion.

SN 1978K lies in the nearby late-type barred spiral galaxy NGC 1313. This appears to be an isolated galaxy at a distance of only ∼4.4–4.6 Mpc (Jacobs et al. 2009; Qing et al. 2015). It has undergone vigorous irregular star formation, driven in part by the action of numerous H I supershells (Ryder et al. 1995). The disk is inclined at 48° to the line of sight—permitting an excellent view of the whole galaxy—and the diffuse X-ray emission is low; this has allowed detailed studies of its point sources.

As the supernova blast wave expands, we can study (on a human timescale) how the wind from the massive progenitor evolved in its final hundreds and thousands of years. Besides being historically interesting, SN 1978K has many intriguing properties in its own right.

The peak radio luminosity was very high; at its peak, SN 1978K would have been one of the most luminous radio supernovae ever. SN 1978K is thus one of the most important members of the "Type IIn" sub-class of supernovae, (e.g., Schlegel 1990; Schlegel et al. 2000; Gal-Yam et al. 2007; Smith et al. 2007b; Bauer et al. 2008; Chandra et al. 2012a, 2012b). Type IIn events make up ∼10% of all core-collapse supernovae (Smith et al. 2011).

In Ryder et al. (2016), we showed a radio VLBI image from 2015 March 29 at 8.4 GHz. This revealed that the source remains compact—with a <5 mas (0.11 pc) diameter—allowing us to place an upper limit on the average expansion velocity of 1500 km s^{-1}. This is consistent with there being a dense circumstellar medium surrounding the progenitor star.

The optical spectrum of SN 1978K is dominated by emission lines that are only moderately broad, unlike most supernova ejecta (Ryder et al. 1993; Chugai et al. 1995; Chu et al. 1999; Kuncarayakti et al. 2016). This also shows that the surrounding medium was dense, causing a rapid slowdown of the shock. The possibility of a strong wind from the progenitor led to the suggestion that it was a luminous blue variable (Chu et al. 1999; Gruendl et al. 2002; Gal-Yam et al. 2007; Kiewe et al. 2012). Although no pre-explosion imaging is available that might have allowed the progenitor properties to be determined, age-dating of the stellar population surrounding SN 1978K using the *Hubble Space Telescope* suggests a progenitor mass of 8.8 ± 0.2 $M_\odot$ (Williams et al. 2018).

Kuncarayakti et al. (2016) compared SN 1978K spectra taken from 1990 through 2014 and found that different lines evolved differently. This suggests the evolution is not spherically symmetric, similar to SN 1987A.

While the radio flux dropped steadily, the X-ray and UV/optical fluxes for SN 1987K remained surprisingly constant from 2000 to at least 2008 (Smith et al. 2007a). Starting in

Table 1
ALMA Millimeter Observations of SN 1978K in 2016

Band Number	UT Date (YYYY-MM-DD)	MJD	Age[a] (days)	Time on Science Target (min)	Maximum Baseline (km)	Precipitable Water Vapor (mm)	Average Source Elevation (degrees)
3	2016 Sep 2	57633	13983	16.7	1.8	1.38	42.4
4	2016 Jul 25	57594	13944	21.2	1.1	0.94	45.9
6	2016 Jun 9	57549	13899	26.8	0.7	1.23	45.5
7	2016 Jun 16	57556	13906	70.4	0.8	0.72	44.1

Note.
[a] Age based on the adopted explosion date of 1978 May 22 (MJD 43650).

2013, our X-ray, UV, and optical observations finally revealed these were fading, but with chromatic variability (Zhao et al. 2017, I. A. Smith 2019, in preparation). As noted by Dwarkadas & Gruszko (2012), many SN Type IIn light curves do not show the simple decaying X-ray luminosity that would be expected from a blast wave expanding into a steady wind.

Over many years, we have been performing detailed radio through X-ray observations of SN 1978K (Smith et al. 2007a; Ryder et al. 2016; I. A Smith 2019, in preparation). In this paper, we focus on new millimeter observations made by the Atacama Large Millimeter/submillimeter Array (ALMA), radio observations made by the Australia Telescope Compact Array (ATCA), and infrared observations made by the *Spitzer Space Telescope* (*Spitzer*). In Section 2, we present the ALMA millimeter observations of SN 1978K from 2016, updated ATCA radio light curves, and *Spitzer* infrared light curves and a spectrum. In Section 3, we use two different models to explain the combined radio-millimeter synchrotron spectrum. In Section 4, we discuss the implications of the new observations on the warm and cold dust emission in SN 1978K. In Section 5, we outline how future observations might reveal more information about the source.

2. Observations and Results

2.1. 2016 ALMA Observations of SN 1978K

Only three extragalactic supernovae have been detected at late times at millimeter wavelengths: SN 1978K, SN 1987A (Matsuura et al. 2011, 2015; Lakićević et al. 2012), and SN 1996cr (Meunier et al. 2013). SN 1978K was first detected at 34 and 94 GHz in our ATCA observations in 2014 September (Ryder et al. 2016). SN 1987A is only detectable because it is nearby; at the distance of SN 1978K, it would not be detectable by ALMA. This highlights the danger of extrapolating the SN 1987A results to other supernovae, and shows the importance of studying other luminous supernovae.

During Cycle 3 in 2016, ALMA observed SN 1978K in Bands 3, 4, 6, and 7. Details of the observations are given in Table 1. SN 1978K was observed at a good elevation in all four bands. The weather conditions were stable during all the observations. The sources J0519–4546 (Bands 3, 4, and 6), J2258–2758 (Band 7), and J0538–4405 (Band 7) were used as bandpass calibrators; J0334–4008 (Band 3), J0519–4546 (Bands 4 and 6), and Ceres (Band 7) were used as amplitude calibrators; and J0303–6211 was the phase calibrator for all the observations.

All the observations were reprocessed using the complete calibration pipeline in CASA version 4.7.2 (McMullin et al. 2007). Multi-frequency synthesis with the multi-term (multi scale) multi-frequency synthesis (mtmfs) deconvolver was used when combining channels to make continuum images; nterms = 2 was used, which assumes a simple sloped spectrum. The images were cleaned using the task TCLEAN with a Briggs weighting and `robust = 0.5`. Primary beam corrections were applied on the restored images. The observations were short, and the source was not bright enough to merit doing phase or amplitude self-calibration.

SN 1978K was well detected in the observations in all four bands. The background around the source was smooth. SN 1978K was consistent with being point-like in all the observations.

Each ALMA band is split into four spectral windows (SPWs) of bandwidth 1.875 GHz. Each SPW contains 128 channels. No obvious lines were found in addition to the continuum. Thus all the good channels were combined to obtain the continuum fluxes in the four separate SPWs. These results are shown in Table 2 and as the black points in Figure 1.

The gold points in Figure 1 combine the SPWs in pairs; there is only a small difference in the frequencies for the two lower SPWs and for the two higher SPWs, making these combinations robust.

The magenta points in Figure 1 combine all the SPWs in each band. There is a larger difference in the frequencies for the lower and higher pairs of SPWs. Given changes in the beam across the broad bands and interpolation concerns, it might be considered a little less robust to combine all the data for the whole band. However, the magenta points show this can be done without any problems.

2.2. Updated ATCA Light Curves for SN 1978K

We have been performing radio monitoring of SN 1978K using the ATCA at irregular intervals since its discovery (Ryder et al. 1993; Schlegel et al. 1999; Smith et al. 2007a).

The Compact Array Broad-band Backend (CABB; Wilson et al. 2011) was commissioned in early 2009. It provides 2 × 2 GHz IF bands, each of which has 2 × 2048 channels of 1 MHz each. This yields a factor of 4 improvement in the continuum sensitivity over the 128 MHz bandwidths used for the observations reported in our previous papers. The band central frequencies are chosen to minimize radio frequency interference across each band, and differ from those shown in our previous work. Details of the ATCA CABB observations are given in Table 3. We remark that some pre-CABB ATCA observations of SN 1978K taken between 2007 November 21 and 2009 January 29 suffered from problems with the phase stability and are not included here.

The ATCA primary flux calibrator, PKS B1934–638, was observed once per run at each frequency to set the absolute flux

Table 2
ALMA Results for SN 1978K in 2016

Band Number	Spectral Window(s)	Center Frequency of Image (GHz) (LSRK)	Beam (arcsec)	Source Flux Density (mJy)	Image rms (mJy/beam)
3	17	90.4832	0.66 × 0.46	1.451 ± 0.083	0.048
	19	92.4286	0.64 × 0.47	1.660 ± 0.120	0.065
	21	102.5150	0.58 × 0.40	1.314 ± 0.077	0.045
	23	104.5073	0.57 × 0.40	1.284 ± 0.067	0.044
	17 + 19	91.2567	0.65 × 0.46	1.561 ± 0.070	0.041
	21 + 23	103.5151	0.57 × 0.40	1.289 ± 0.054	0.031
	All 4	97.4992	0.59 × 0.42	1.412 ± 0.047	0.025
4	17	138.1083	0.57 × 0.41	0.890 ± 0.051	0.032
	19	139.9364	0.56 × 0.43	0.920 ± 0.055	0.029
	21	150.0149	0.52 × 0.37	0.794 ± 0.044	0.028
	23	151.9056	0.52 × 0.37	0.812 ± 0.052	0.031
	17 + 19	138.9833	0.55 × 0.41	0.896 ± 0.038	0.022
	21 + 23	150.9055	0.51 × 0.37	0.796 ± 0.036	0.021
	All 4	145.0147	0.52 × 0.39	0.855 ± 0.026	0.015
6	17	223.9891	0.69 × 0.52	0.598 ± 0.079	0.050
	19	225.9892	0.68 × 0.51	0.636 ± 0.099	0.046
	21	240.0207	0.63 × 0.47	0.404 ± 0.071	0.052
	23	242.0207	0.63 × 0.46	0.580 ± 0.159	0.059
	17 + 19	224.9891	0.67 × 0.51	0.616 ± 0.070	0.035
	21 + 23	241.0207	0.62 × 0.46	0.437 ± 0.069	0.040
	All 4	233.0049	0.63 × 0.48	0.525 ± 0.050	0.026
7	0	336.5019	0.37 × 0.30	0.407 ± 0.139	0.060
	1	338.4394	0.37 × 0.30	0.583 ± 0.110	0.053
	2	348.5021	0.36 × 0.29	0.450 ± 0.138	0.056
	3	350.5022	0.36 × 0.29	0.436 ± 0.112	0.065
	0 + 1	337.4706	0.37 × 0.30	0.500 ± 0.093	0.042
	2 + 3	349.5022	0.36 × 0.29	0.435 ± 0.092	0.043
	All 4	343.5020	0.36 × 0.29	0.458 ± 0.066	0.030

scale, as well as define the bandpass calibration in each band. Frequent observations of the nearby source PKS 0302–623 allowed us to monitor and correct for variations in gain and phase throughout each run.

The data were processed using the Miriad package (Sault et al. 1995) and using procedures outlined in Section 4.3 of the ATCA User Guide.[6] After editing and calibrating the data, images at each frequency were made using robust weighting (`robust = 0.5`), then cleaned down to 3× the rms. noise level. The "16 cm" band covers 1.1–3.1 GHz, or a factor of 3 in beam size, so it has to be divided into 4 sub-bands of 512 MHz each in order to be processed properly. Fitting a Gaussian point source at the location of SN 1978K yielded the flux densities shown in Table 3 and Figure 2. The uncertainty in each case is a combination of the fitting and absolute flux calibration errors.

2.3. Spitzer Observations of SN 1978K

Spitzer observations of younger supernovae (age < 10 yr) have shown that Type IIn can initially be bright in the mid-infrared (e.g., Szalai et al. 2018).

Tanaka et al. (2012) used *Spitzer* and *AKARI* to study six supernovae in the "transitional" phase (age 10–100 yr). Only SN 1978K was detected, in 2006. This is suggestive of emission from warm (a few 100 K) dust.

Since 2006, the InfraRed Array Camera (IRAC) on *Spitzer* (Fazio et al. 2004; Werner et al. 2004) has continued to make observations of NGC 1313 in both the cryogenic and post-cryogenic phases; a few of these observations have had SN 1978K in the field of view. Details of the observations are given in Table 4.

The IRAC observations were processed using the most recent *Spitzer* pipelines; these were versions S18.25 for the cryogenic observations (prior to 2009 May) and S19.2 for the post-cryogenic observations. SN 1978K was well detected in all four channels. The surrounding background is fairly smooth and free from other sources. Point-source photometry was performed on the Corrected Basic Calibrated Data generated by the pipeline using APEX in the MOPEX package (Makovoz & Marleau 2005). Short exposure frames were dropped from the mosaicking. Location-dependent photometric corrections that are often applied to bluer stars were not used for SN 1978K because it is a very red source. A point response function (PRF) map was used in APEX Multiframe to improve the fitting for sources outside the central region. Correction factors for the PRF flux densities were taken from Table C1 of the IRAC Instrument Handbook version 2.1.2.

The *Spitzer* IRAC light curves for SN 1978K are shown in Figure 3 and reveal a rapid fading of the source. The fluxes of other nearby stars of similar brightness were consistent with remaining constant over the decade (to within the expected few percent uncertainties).

[6] http://www.narrabri.atnf.csiro.au/observing/users_guide/html/atug.html

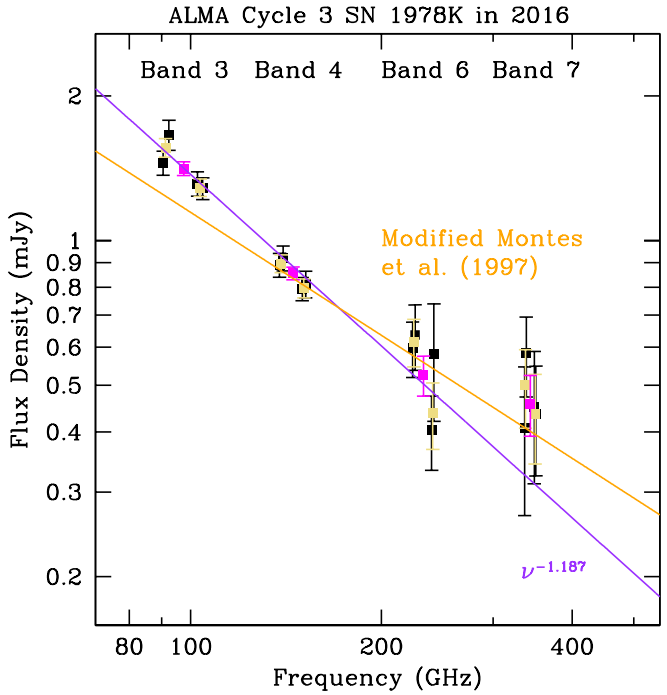

Figure 1. Cycle 3 ALMA observations of SN 1978K in 2016. The black points show the four separate spectral windows for each band. The gold points combine the spectral windows in pairs, and the magenta points combine all the data for each band. The orange curve shows the modified version of the Montes et al. (1997) model described in Section 3.1. The purple curve shows the $\nu^{-1.187}$ power law appropriate for an ultra-relativistic spherical blast wave with a wind scaling above the cooling break that is described in Section 3.2.

On 2008 July 7 (MJD 54654, AOR 26536704), the InfraRed Spectrograph (IRS) on *Spitzer* (Houck et al. 2004) made cryogenic observations pointed at SN 1978K using the Staring Mode in Channel 0 (Short-Low) and Channel 2 (Long-Low). The IRS enhanced spectrophotometric products were produced, starting with the cryogenic pipeline S18.18 processed spectra, and merged using IRS MERGE v2.1 to produce the spectrum SPITZER_S5_26536704_01_merge.tbl in the *Spitzer* Heritage Archive. Data that were flagged as questionable were removed.

The *Spitzer* IRS mid-infrared spectrum is shown in Figure 4; see also van Dyk (2011). The double-peaked spectrum is broadly consistent with the *AKARI* observations and modeling shown in Tanaka et al. (2012).

3. Radio-millimeter Spectral Modeling

Figure 5 combines the radio and millimeter observations of SN 1978K, and shows model fits from two possible interpretations for the radio-millimeter spectrum.

3.1. Montes et al. (1997) Model

Based on the model of Weiler et al. (1986, 1990) and the early observations of SN 1978K, Montes et al. (1997) generated a parameterized model for a supernova shock interacting with a high-density ionized circumstellar envelope. The model is described in detail in Montes et al. (1997) and Schlegel et al. (1999). This effectively has a single power-law spectral index α at high frequencies with attenuation at lower frequencies from the intervening medium. The main temporal decay power-law index β is independent of the frequency; $\beta = -1.53$ as shown in the radio decay in Figure 2. The initial unabsorbed flux density normalization at 5 GHz is given by K_1. There is absorption from local uniform and local non-uniform material with initial optical depths at 5 GHz given by K_2 and K_3 and power-law temporal decay indices $\delta \equiv \alpha - \beta - 3$ and $\delta' \equiv 5\delta/3$, respectively. There is also a "distant" absorption that is assumed to be time-independent whose optical depth at 5 GHz is given by K_4. All the absorbing media are assumed to be purely thermal ionized hydrogen, with the opacities having a $\nu^{-2.1}$ dependence.

In Figure 2 of Ryder et al. (2016) we modeled the 2014 ATCA radio and millimeter observations out to 94 GHz using a modified version of the Montes et al. (1997) model. The extension to higher frequencies with the ALMA data necessitated additional tweaking of the model parameters. The full set of parameters used is given in Table 5.

As shown in Figure 6(a), at early times the updated Montes et al. (1997) model gives a radio evolution that is very similar to that shown in Figure 10 of Schlegel et al. (1999). As noted in Schlegel et al. (1999), this model does not have a good explanation for the flat initial light curve at 1.4 GHz.

The updated Montes et al. (1997) model is compared to the more recent ATCA and ALMA observations described in Section 2 using the solid orange curve in Figures 1 and 5 and the solid colored curves in Figure 2. It provides a decent general description of all the recent radio and millimeter observations of SN 1978K.

However, the 2013 June 07 ATCA observation appears to have a dip at the four lower frequencies, but not at the two higher ones; the data points lie 3.0σ, 4.7σ, 4.7σ, and 5.1σ below the Montes et al. (1997) model curves at 1.33 GHz, 1.84 GHz, 2.36 GHz, and 2.87 GHz, respectively. The deviation at the lower frequencies went away by 2018 March 19.

Chromatic fluctuations might be the result of inhomogeneities in the radio-emitting region, implying there were fluctuations in the mass-loss rate of the progenitor star as recently as a few hundred years before the explosion.

Compact extragalactic radio sources can also appear to vary as a result of interstellar scintillation (Walker 1998). SN 1978K is at a galactic latitude of $-44.^{\circ}7$. For this latitude, the transition frequency at which the scattering strength is unity is $\nu_0 \sim 4.5$ GHz. Thus, this lies in the middle of our range of ATCA radio frequencies. At this galactic latitude, the angular size limit of the first Fresnel zone for an extragalactic source being observed at ν_0 is $\theta_{\rm F0} \sim 5 \times 10^{-6}$ arcsec. Sources (or components thereof) that are smaller than this size limit can be approximated as point sources and may show deep modulations in their received flux. Our VLBI imaging at 8.4 GHz shows that SN 1978K is <5 mas in diameter. Thus scintillation could be responsible for a larger variability at the lower frequencies if SN 1978K extends over microarcsecond scales rather than milliarcsecond scales.

Figure 1 shows that the four independent Band 3 ALMA SPW all lie well above the Montes et al. (1997) model curve. The combined data for the whole of Band 3 lies 5.2σ above the model. Thus, the Montes et al. (1997) model would need significant chromatic fluctuations in the millimeter to explain the excess in 2016.

3.2. Broken Power-law Fireball Model

Figure 1 indicates that the millimeter spectrum on its own might be better explained using a steeper power-law index than the one used for the radio. Figure 5 shows that for a broken

Table 3
ATCA CABB Radio Observations of SN 1978K

UT Date (YYYY-MM-DD)	MJD	Age[a] (days)	Array	Flux Densities (mJy)					
				1.33 GHz	1.84 GHz	2.36 GHz	2.87 GHz	5.50 GHz	9.00 GHz
2009 Oct 9	55114	11464	H75C	...	...	...	...	19.2 ± 2.2	10.5 ± 3.3
2009 Oct 13	55118	11468	H168C	...	...	37.6 ± 6.2	...	...	...
2013 Jun 7	56451	12801	6C	31.4 ± 2.7	26.1 ± 1.7	23.0 ± 1.3	20.7 ± 0.9	15.1 ± 0.8	10.7 ± 0.5
2017 Sep 4	58001	14351	1.5A	...	...	...	...	12.1 ± 0.5	8.4 ± 0.5
2018 Mar 19	58197	14547	EW352	35.7 ± 4.7	27.6 ± 1.4	22.2 ± 1.3	18.6 ± 2.5	12.3±0.6	8.5 ± 1.0

Note.
[a] Age based on the adopted explosion date of 1978 May 22 (MJD 43650).

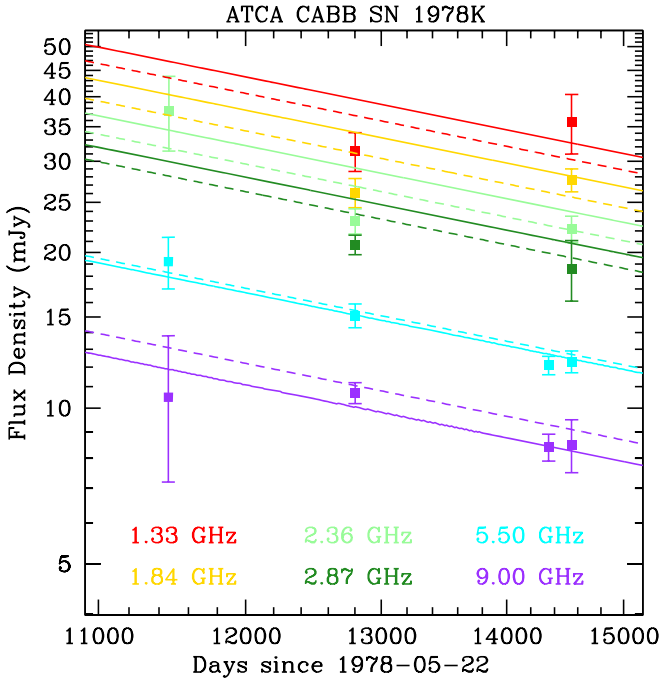

Figure 2. Radio light curves for SN 1978K from Australia Telescope Compact Array monitoring using the Compact Array Broad-band Backend between 2009 and 2018. From top to bottom, these are at 1.33 GHz (red), 1.84 GHz (gold), 2.36 GHz (light green), 2.87 GHz (dark green), 5.50 GHz (cyan), and 9.00 GHz (purple). The solid curves show the evolution given by the modified version of the Montes et al. (1997) model described in Section 3.1; this asymptotes to a $t^{-1.53}$ power law at late times for all the frequencies. The dashed curves use the absorbed ultra-relativistic spherical blast wave with a wind scaling model described in Section 3.2: $A = 90.3$, $B = 3.287 \times 10^5$, and $K_4 = 7.0 \times 10^{-3}$. 1978 May 22 was MJD 43650.

power-law model, the change in the spectral index appears to be ∼0.5.

In a gamma-ray burst (GRB) afterglow spectrum, a change of 0.5 in the spectral index is expected for a cooling break in the late-time emission from an ultra-relativistic spherical blast wave (e.g., Granot & van der Horst 2014). In Smith et al. (2007a) we showed that SN 1978K was inside the $\sim 4\sigma$ error box of GRB 771029. The quality of the GRB locations at that time was poor, and this may just have been a chance alignment. Type IIn supernovae are not generally expected to produce GRBs, and this would have been a very underluminous burst at the distance of NGC 1313. However, we can still adopt the generic fireball formalism here.

In the GRB fireball model with a wind scaling for the external medium, frequencies below the cooling break (ν_c) will have a temporal decay of $t^{(1-3p)/4}$, where p is the electron spectral index. Using our observed radio decay of $t^{-1.53}$ from Figure 2, this implies $p = 2.373$.

The fireball model then requires that the spectral indices be $\nu^{(1-p)/2} = \nu^{-0.687}$ below ν_c and $\nu^{-p/2} = \nu^{-1.187}$ above it. As shown by the cyan and purple curves in Figures 1 and 5, these spectral indices naturally explain the observed radio-millimeter spectrum. The fact that both the radio temporal decay and the spectral indices independently agree with the fireball expectations make this a promising interpretation.

The $\nu^{-0.687}$ and $\nu^{-1.187}$ power laws are the asymptotic spectral indices. In theory, the spectrum could have a sharp break if there is a unique cooling frequency. In practice, it is usually assumed that there is a smooth transition between the two power laws. This would then explain why the 34 GHz ATCA point lies below the cyan curve in Figure 5.

A GRB fireball model with an ISM scaling for the external medium does not explain the SN 1978K observations. In this case, the frequencies below ν_c would have a temporal decay of $t^{3(1-p)/4} = t^{-1.53}$, giving $p = 3.04$. The spectral indices would then be $\nu^{(1-p)/2} = \nu^{-1.02}$ below ν_c and $\nu^{-p/2} = \nu^{-1.52}$ above it: these are both steeper than those in our radio and millimeter observations.

Two additional breaks in the spectrum are involved in explaining the radio emission at early times in the fireball model with a wind scaling for the external medium: the peak frequency ν_m (which corresponds to the minimum energy of the electron energy distribution), and the synchrotron self-absorption frequency ν_{sa}. The case where $\nu_{sa} < \nu_m < \nu_c$ can be used to explain the radio evolution of SN 1978K. In a snapshot of the spectrum, the flux rises as ν^2 up to ν_{sa}, breaks to $\nu^{1/3}$ up to ν_m, falls as $\nu^{-0.687}$ up to ν_c, and falls as $\nu^{-1.187}$ beyond ν_c. The four segments of the spectrum have different temporal evolutions: t^1 up to ν_{sa}, t^0 between ν_{sa} and ν_m, $t^{-1.53}$ between ν_m and ν_c, and $t^{(2-3p)/4} = t^{-1.280}$ above ν_c. The three characteristic frequencies are also not static, with temporal evolutions $\nu_{sa} = A\ (t - t_0)^{-3/5}$, $\nu_m = B\ (t - t_0)^{-3/2}$, and $\nu_c = C\ (t - t_0)^{1/2}$.

From Figure 5, $\nu_c = 54.55$ GHz at $(t - t_0) = 13934$ days, giving $C = 0.4621$. The flux density of 2.820 mJy at this time and this frequency fixes the overall normalization.

Figure 6(b) shows the radio evolution of the fireball model at early times using $A = 88.8$ and $B = 3.727 \times 10^5$. Unlike the Montes et al. (1997) model, the fireball model naturally explains how the flux at 1.4 GHz remained constant when $\nu_{sa} < 1.4$ GHz $< \nu_m$, while at the same time the flux at 0.8 GHz was rising as t^1 because 0.8 GHz $< \nu_{sa}$. While this is promising independent evidence favoring the fireball model, we caution that scintillation may be an issue at lower

Table 4
Spitzer IRAC Infrared Observations of SN 1978K

UT Date (YYYY-MM-DD)	MJD	Age[a] (days)	AOR	Flux Densities (mJy)			
				3.6 μm	4.5 μm	5.8 μm	8.0 μm
2007 Sep 12	54356	10706	22524160[b]	0.05764 ± 0.00124	0.10620 ± 0.00130	0.1831 ± 0.0065	0.7347 ± 0.0072
2008 Jun 10	54627	10977	26537216	0.05353 ± 0.00180	0.09883 ± 0.00262	0.1796 ± 0.0103	0.6971 ± 0.0129
2011 Jul 7	55749	12099	42193408	0.04475 ± 0.00188	0.07783 ± 0.00132	⋯	⋯
2012 Feb 1	55959	12309	42193152	0.04169 ± 0.00195	0.07623 ± 0.00126	⋯	⋯
2014 Feb 12	56701	13051	50504704	⋯	0.07168 ± 0.00205	⋯	⋯
2016 Aug 5	57606	13956	52691456	0.03138 ± 0.00083	⋯	⋯	⋯
2017 Jan 2	57755	14105	60812544	⋯	0.05311 ± 0.00063	⋯	⋯
2018 Feb 9	58158	14508	60813568	⋯	0.05132 ± 0.00065	⋯	⋯
2018 Aug 24	58355	14705	66130688	0.02500 ± 0.00068	0.04858 ± 0.00058	⋯	⋯

Notes.
[a] Age based on the adopted explosion date of 1978 May 22 (MJD 43650).
[b] Combines AOR 22524160 and 22524416.

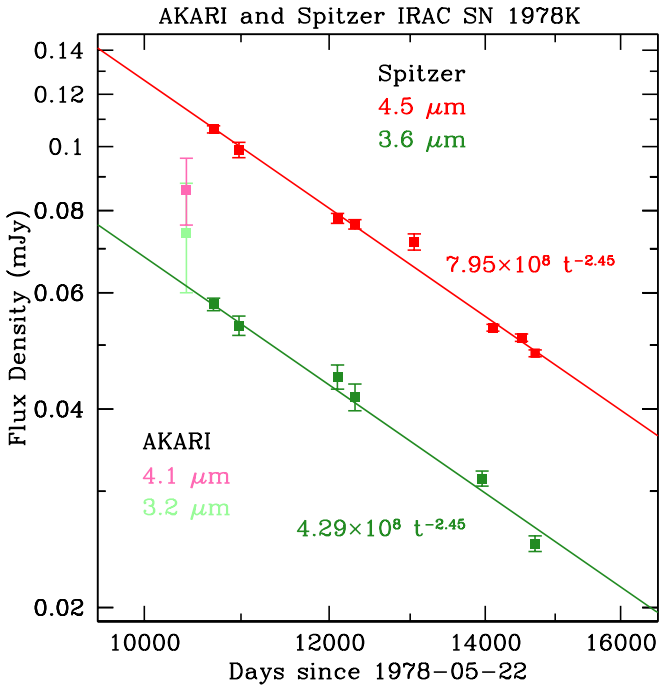

Figure 3. Infrared light curves for SN 1978K at 4.5 μm (red, upper) and 3.6 μm (dark green, lower) from *Spitzer* IRAC observations from 2007 to 2018. A $t^{-2.45}$ power-law decay is shown for both channels. The 2006 December 3–4 *AKARI* observations (Tanaka et al. 2012) are included for comparison, although these use different wavelength bands: 4.1 μm (pink, upper) and 3.2 μm (light green, lower). 1978 May 22 was MJD 43650.

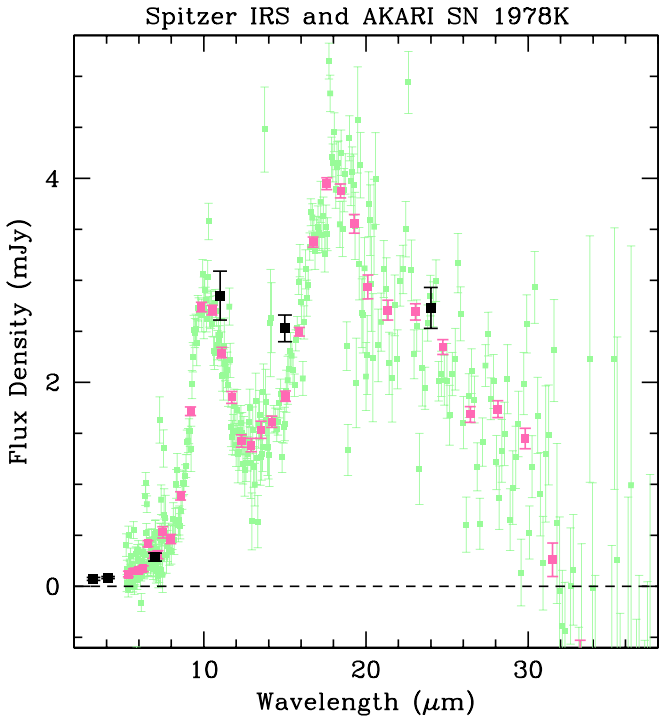

Figure 4. Mid-infrared spectrum of SN 1978K taken on 2008 July 07 by the *Spitzer* IRS using the full spectral resolution (light green) and re-binned using weighted means to combine every 10 data points (pink). The 2006 December 3–4 *AKARI* observations (Tanaka et al. 2012) are included for comparison (black).

frequencies, there may be chromatic variability in the radio, and there may have been problems with the calibration or background subtraction in some of the early observations.

Figure 6(b) shows the pure unabsorbed radio emission from the fireball. It appears to produce more than the observed flux at the lower frequencies. The same problem was found in the Montes et al. (1997) model, which motivated including a time-independent and frequency-dependent absorption from material that is "distant" from the source. The same $e^{-\tau''}$ attenuation can be applied to the fireball model, where $\tau'' = K_4\,(\nu\,/\,5\,\mathrm{GHz})^{-2.1}$ as in Montes et al. (1997). Figure 6(c) shows an example of an absorbed fireball with $A = 90.3$, $B = 3.287 \times 10^5$, and $K_4 = 7.0 \times 10^{-3}$: this appears to give a better description of the early radio evolution, albeit with the same caveats regarding the early radio observations at low frequencies.

For our recent ATCA and ALMA observations, the absorbed fireball model is shown as the dashed curves in Figures 2 and 5. The 2013 June 7 ATCA data points lie 2.0σ, 3.0σ, 3.0σ, and 3.4σ below the absorbed fireball model curves at 1.33 GHz, 1.84 GHz, 2.36 GHz, and 2.87 GHz respectively. Thus, these are much less discrepant than those for the Montes et al. (1997) model, and there is less need to invoke chromatic variability in the absorbed fireball model.

4. Dust Implications

Enormous amounts of dust (up to $10^8\,M_\odot$) have been found in high-redshift ($z \gtrsim 6$) galaxies from a variety of far-infrared and submillimeter observations (e.g., Pei et al. 1991; Pettini et al. 1997;

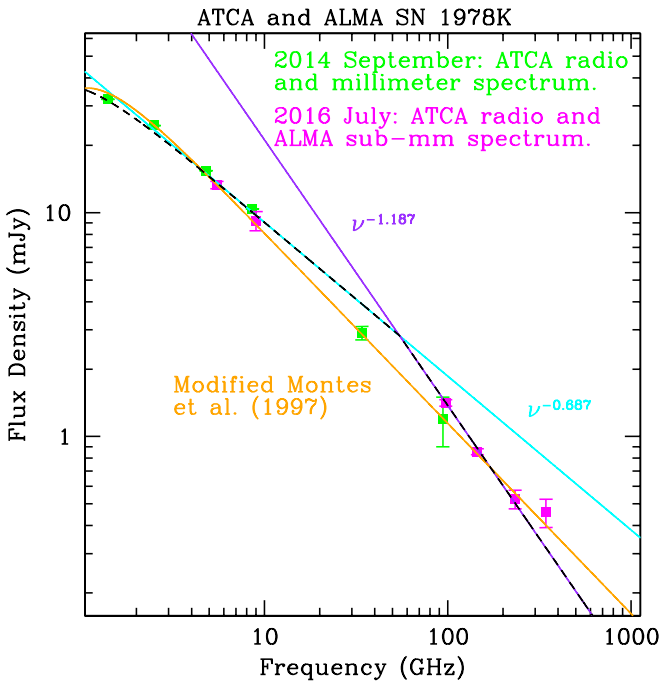

Figure 5. The green points reproduce Figure 2 of Ryder et al. (2016), and show our ATCA millimeter observations from 2014 September along with the radio spectrum extrapolated to that time. The magenta points show our 2016 ALMA observations for the full bands along with ATCA radio points interpolated to that time. The orange curve shows the modified version of the Montes et al. (1997) model described in Section 3.1. The power laws show an unabsorbed ultra-relativistic spherical blast wave with a wind scaling below the cooling break ($\nu^{-0.687}$; cyan), and above the cooling break ($\nu^{-1.187}$; purple) as described in Section 3.2. The black dashed curve uses the absorbed ultra-relativistic spherical blast wave with a wind scaling model described in Section 3.2: $A = 90.3$, $B = 3.287 \times 10^5$, and $K_4 = 7.0 \times 10^{-3}$.

Table 5
Montes et al. (1997) Model Parameters Used for SN 1978K in 2016

Parameter	Value
α	−0.85
β	−1.53
δ	−2.32
δ'	−3.87
$t - t_0$	13934
K_1	3.2×10^7 mJy
K_2	4.0×10^4
K_3	3.6×10^{11}
K_4	1.6×10^{-2}

Laporte et al. 2017). However, the source of this dust remains unclear, with several possible contributors.

The short timescales required for dust enrichment make core-collapse supernovae rather natural candidates for dust producers in the early universe. Estimates of the amount of dust produced per supernova are sensitive to the choice of the initial mass function and the grain destruction efficiencies; it is likely that each supernova must produce 0.1–1 $M_\odot$ of dust to account for the high-redshift observations (e.g., Dwek et al. 2007; Meikle et al. 2007).

Studies of young supernovae a few hundred days after their explosion have tended to find dust masses that are much too low (e.g., Kotak et al. 2009; Andrews et al. 2011; Meikle et al. 2011), although the amount of dust may still be rising at this stage (Sarangi & Cherchneff 2013). On the other hand, studies of old supernova remnants have the problem of the dust grains being destroyed by the reverse shock as the ejecta interacts with the ambient medium (e.g., Nozawa et al. 2006; Williams et al. 2006).

Thus, it is of particular interest to look for dust in supernovae in the transitional phase that have not transitioned fully into the remnant phase. This ensures that ISM material has not been swept up by the ejecta, and that the emission is due to material directly associated with the progenitor system.

4.1. Warm Dust in SN 1978K

The *Spitzer* IRAC light curves in Figure 3 show that SN 1978K has faded steadily since the 2006 *AKARI* observation. This proves that this emission is coming from SN 1978K, and not from an unrelated dust cloud in the same direction.

Figure 7 updates Figure 2 of Tanaka et al. (2012). The *AKARI* infrared points show SN 1978K on 2006 December 3–4. The model curves from Figure 5 have been extrapolated back to this time. For the Montes et al. (1997) model, the evolution is $t^{-1.53}$ for all frequencies. For the fireball model, the evolution is $t^{-1.53}$ below ν_c and $t^{-1.28}$ above it. The ALMA and ATCA data points from Figure 5 have been extrapolated back assuming the fireball evolution.

Tanaka et al. (2012) used a $\nu^{-0.60}$ power law—shown as the dotted red curve in Figure 7—to extrapolate from the radio to explain the shortest wavelength infrared emission at 3.2 and 4.1 μm. Instead, our ATCA and ALMA observations show that the radio-millimeter spectrum is much steeper than this. Thus, the contribution from synchrotron radiation to the infrared emission is much smaller than what was assumed by Tanaka et al. (2012).

Tanaka et al. (2012) preferred a model that used 1.3×10^{-3} $M_\odot$ of silicate dust at $T = 230$ K. This gives a double-peaked spectrum similar to the *Spitzer* IRS one shown in Figure 4. Removing the synchrotron component, the increase in the peak flux that needs to come from warm dust is relatively small, $\lesssim$10%. However, there is a much greater impact on the shape of the spectrum. The favored silicate model shown in Figure 3 of Tanaka et al. (2012) is too narrow, with insufficient emission at 3.2 and 4.1 μm. Instead, the amorphous carbon model with 6.8×10^{-3} $M_\odot$ of dust at $T = 180$ K has a broader shape that could explain both the 3.2 and 4.1 μm emission and the longer wavelength emission, but which fails to provide the peak at $\sim$10 μm. This suggests that multiple dust emission components may be involved.

Figure 3 shows that over the past decade, the fluxes at 3.2 and 4.1 μm have dropped by a factor of $\sim$2. The $t^{-2.45}$ power-law decay in both channels is much faster than we have found in the radio ($t^{-1.53}$, Figure 2), optical, UV, or X-rays. Since multiple dust emission components may be present, it should be noted that it is only the very warmest dust that is known to be fading.

The rapid decay at 3.2 and 4.1 μm indicates this is not a simple geometric expansion of the emitting region. Figure 3 showed that the decay rate is the same in both infrared channels; this indicates that it is not the result of a cooling of the dust. The simplest explanation is that dust is being destroyed.

Tanaka et al. (2012) preferred a forward-shocked circumstellar dust model for the warm dust emission from SN 1978K, similar to SN 1987A. They claimed that an infrared echo

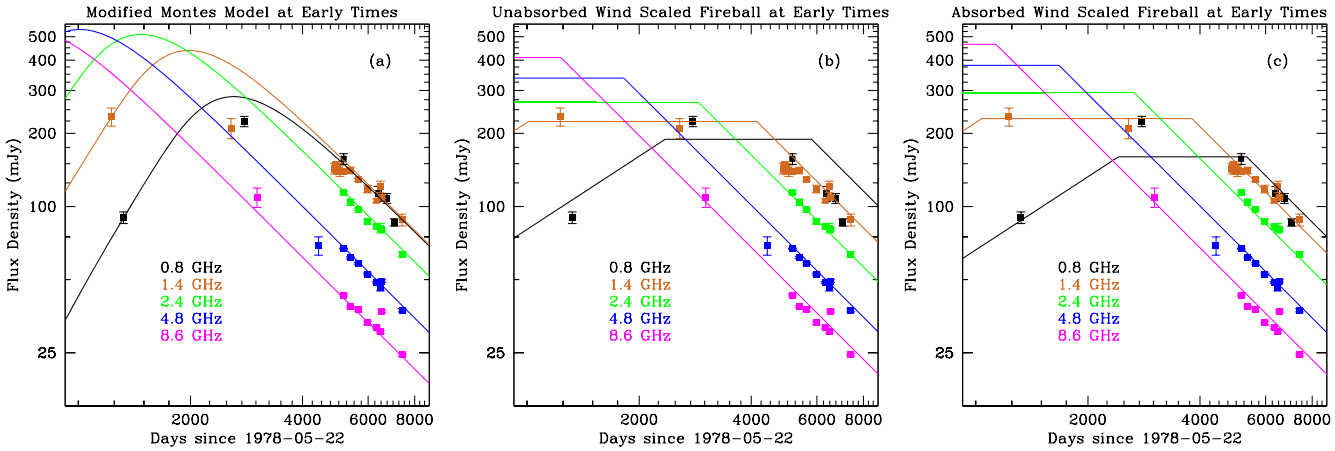

Figure 6. Early radio light curves for SN 1978K at 0.8 GHz (black), 1.4 GHz (brown), 2.4 GHz (green), 4.8 GHz (blue), and 8.6 GHz (magenta). The data are the same as those shown in Figure 10 of Schlegel et al. (1999), which includes additional observations from Ryder et al. (1993), Peters et al. (1994), and Montes et al. (1997). (a) The curves use the modified version of the Montes et al. (1997) model described in Section 3.1. (b) The curves use the unabsorbed ultra-relativistic spherical blast wave with the wind scaling model described in Section 3.2: $A = 88.8$, $B = 3.727 \times 10^5$, and $K_4 = 0$. (c) The curves use the absorbed ultra-relativistic spherical blast wave with the wind scaling model described in Section 3.2: $A = 90.3$, $B = 3.287 \times 10^5$, and $K_4 = 7.0 \times 10^{-3}$.

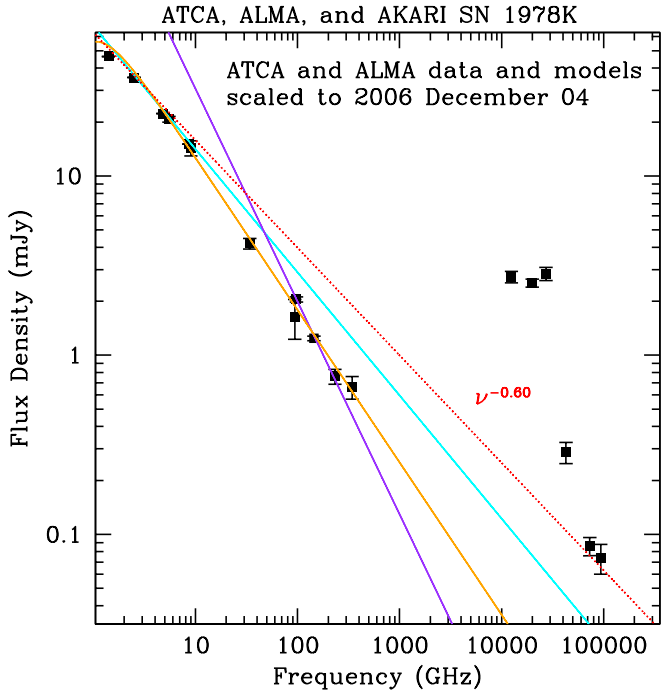

Figure 7. The *AKARI* infrared points show SN 1978K on 2006 December 3–4 (Tanaka et al. 2012). The model curves and ALMA and ATCA data points from Figure 5 have been extrapolated back to this time. The dotted red $\nu^{-0.60}$ power law was previously used by Tanaka et al. (2012) to explain their shortest wavelength observations.

model is unlikely, stating there is not enough energy for this. However, they only considered an initial input of energy, assuming the supernova luminosity had an exponential decay with a characteristic time of 25 days. We have instead shown that SN 1978K has been a strong emitter of UV and X-rays for decades (Smith et al. 2007a). The X-ray energization alone ($\sim 3 \times 10^{39}$ erg s^{-1}) exceeds the infrared luminosity observed ($\sim 1.5 \times 10^{39}$ erg s^{-1}). SN 1978K was first detected by *ROSAT* 13 years after the explosion. It has emitted a total of $\gtrsim 10^{48}$ erg just in 0.2–10 keV X-rays since then. Given the dense medium around SN 1978K, an infrared echo model might still be relevant. However, it is still challenging to explain the different temporal decays in the infrared and X-rays.

4.2. Cold Dust in SN 1978K

Depending on the modeling of the synchrotron emission, it is possible that there is also a significant emission from cold dust in SN 1978K.

Figure 1 shows that the Band 7 ALMA observations can be fully explained using the Montes et al. (1997) model. If this is the correct formalism then there is no indication of any upturn in the spectrum at higher frequencies from a cold dust component.

On the other hand, the fireball model seems to give a better description of the ALMA Band 3, 4, and 6 observations. Figure 1 shows that the Band 7 ALMA observations lie a little above the $\nu^{-1.187}$ fireball curve. Thus, if the fireball model is the correct formalism then there is a suggestion that there may be an upturn in the spectrum at higher frequencies from a cold dust component.

5. Conclusions and Future Work

We have shown that SN 1978K remains bright at longer wavelengths 40 years after its explosion.

Using updated ATCA light curves, we showed that, in general, the radio continues to decay as $t^{-1.53}$.

Our ALMA observations in 2016 show that the spectrum appears to be steeper at higher frequencies. Two models can broadly explain all the radio and millimeter observations. The Montes et al. (1997) model would require significant chromatic variability to explain the details. Alternatively, an ultra-relativistic spherical blast wave in a wind scaling may be a better model. Continued radio and millimeter monitoring could determine the correct model for the synchrotron spectrum by looking for the following features:

1. For the Montes et al. (1997) model to be correct, it is necessary that the current ALMA Band 3 excess comes from a chromatic fluctuation. Thus, it is to be expected that this excess will recede in the next few years.

2. The fireball (or other broken power-law) model predicts that the spectrum will always remain steeper in the millimeter than in the radio, with a distinct change in the spectral slope. Observations in additional millimeter bands and/or with smaller error bars in the individual SPW would better determine the millimeter spectrum.
3. The Montes et al. (1997) model predicts that the asymptotic temporal evolution of the spectrum is frequency-independent ($t^{-1.53}$). The fireball model instead predicts different temporal evolutions below ν_c ($t^{-1.53}$) and above it ($t^{-1.28}$).
4. If interstellar scintillation is causing significant variability in the radio, then the timescale for the variation should be $\sim$ hours to days (Walker 1998). If long radio observations at multiple frequencies reveal different variability at different frequencies, or sub-sets of the channels within a band show different levels of variability, this would indicate that scintillation is important. On the other hand, if the radio variations are the result of inhomogeneities in the radio-emitting region, the timescale for the variations will be much longer and will depend on the mass-loss evolution of the progenitor star.
5. If scintillation is not a problem, then observations at radio frequencies below 1 GHz could determine the shape of the rollover in the spectrum and investigate the contribution of absorption from the distant surrounding medium. The GaLactic and Extragalactic All-sky Murchison Widefield Array (GLEAM) survey (Hurley-Walker et al. 2017) shows a source at the location of SN 1978K with a peak brightness of 94 mJy/beam at 200 MHz. This would be inconsistent with the rollover expected from absorption. At late times, the only significant absorption component remaining in the Montes et al. (1997) model comes from the K_4 term: this is the absorption far from the supernova that is supposed to be time-independent, although in principle this term could be made more complex if the shock is assumed to have passed through part of the "distant" absorbing region. Currently, the large size of the GLEAM beam could include diffuse emission from NGC 1313 and other confusing sources, so higher-resolution observations will be needed to cleanly separate SN 1978K from the host galaxy emission.

Supernovae such as SN 1978K are of particular interest because it has been suggested that they may be important contributors to the universal dust budget. The strong X-ray and UV energization in SN 1978K suggests it might not be a good place to create long-lasting dust. However, SN 1978K does currently have significant emission from warm dust: it was the only supernova in the transitional phase detected by Tanaka et al. (2012).

Our *Spitzer* IRAC light curves show that at least the warmest dust component has been decaying rapidly as $t^{-2.45}$ over the past decade. This suggests this dust is currently being destroyed, although an infrared echo model for the warm dust emission cannot be discounted. Monitoring of the infrared emission—and how it changes with the evolving X-ray and UV fluxes—will be needed to distinguish between the models for the dust emission.

We showed that there is a negligible contribution from synchrotron radiation in the mid-infrared, and thus this emission must all come from warm dust. Currently, the amount of warm dust found in SN 1978K appears to be $< 10^{-2}\ M_\odot$ (Tanaka et al. 2012). Multiple dust emission components may be necessary, and better mid-infrared spectroscopy will be needed to determine the best model for the current composition, temperatures, and masses of the warm dust. This will potentially be possible using the *James Webb Space Telescope*.

Our ALMA observations have not so far revealed a bright emission from cold dust in SN 1978K. However, this is more likely to be detected as an upturn in the spectrum at higher submillimeter frequencies. There is a large gap in frequencies between our 350 GHz ALMA observation and the 12500 GHz *AKARI* one that could potentially hide significant cold dust emission. For example, the purple curves in Figure 10 of Tanaka et al. (2012) showed supernovae dust models with $T = 50$ K; scaling from these to the distance of SN 1978K, 1.0 $M_\odot$ of cool dust would produce a peak of $\sim$1 mJy at $\sim$5000 GHz. Thus, observations in ALMA Bands 8–10 are warranted when these modes have been fully standardized, to look for a significant upturn in the spectrum.

Detailed long-term observations of the decay of SN 1978K will also be important for comparing to other bright supernovae —such as SN 1987A and SN 1996cr—and will serve as a pathfinder for younger Type IIn supernovae.

We thank the referee for some important suggestions.

ALMA is a partnership of ESO (representing its member states), NSF (USA) and NINS (Japan), together with NRC (Canada), *MOST* and ASIAA (Taiwan), and KASI (Republic of Korea), in cooperation with the Republic of Chile. The Joint ALMA Observatory is operated by ESO, AUI/NRAO, and NAOJ. The National Radio Astronomy Observatory is a facility of the National Science Foundation operated under cooperative agreement by Associated Universities, Inc. This paper makes use of the following ALMA data: ADS/JAO. ALMA#2015.1.00869.S (P.I. I. Smith).

The Australia Telescope Compact Array is part of the Australia Telescope National Facility, which is funded by the Australian Government for operation as a National Facility managed by CSIRO. The ATCA data reported here were obtained under Program C184 (P.I. S. Ryder).

This work is based in part on observations made with the *Spitzer Space Telescope*, which is operated by the Jet Propulsion Laboratory, California Institute of Technology under a contract with NASA. The *Spitzer* data reported here were obtained under Programs 10136, 11063, and 13053 (P.I. M. Kasliwal), 40204 (P.I. R. Kennicutt), 50603 (P.I. S. Van Dyk), 80015 (P.I. C. Kochanek), and 14108 (P.I. I. Smith).

S.R. and R.K. acknowledge support from the Royal Society International Exchange scheme (IE140343).

Facilities: ALMA, ATCA, *Spitzer*, *Akari*.

Software: CASA (McMullin et al. 2007), Miriad (Sault et al. 1995), MOPEX (Makovoz & Marleau 2005).

ORCID iDs

I. A. Smith https://orcid.org/0000-0001-8605-5608
S. D. Ryder https://orcid.org/0000-0003-4501-8100
R. Kotak https://orcid.org/0000-0001-5455-3653

References

Andrews, J. E., Sugerman, B. E. K., Clayton, G. C., et al. 2011, ApJ, 731, 47
Bauer, F. E., Dwarkadas, V. V., Brandt, W. N., et al. 2008, ApJ, 688, 1210

Bregman, J. N., Houck, J. C., Chevalier, R. A., & Roberts, M. S. 2003, ApJ, 596, 323
Chandra, P., Chevalier, R. A., Chugai, N., et al. 2012a, ApJ, 755, 110
Chandra, P., Chevalier, R. A., Irwin, C. M., et al. 2012b, ApJL, 750, L2
Chu, Y.-H., Caulet, A., Montes, M. J., et al. 1999, ApJL, 512, L51
Chugai, N. N., Danziger, I. J., & della Valle, M. 1995, MNRAS, 276, 530
Dwarkadas, V. V., & Gruszko, J. 2012, MNRAS, 419, 1515
Dwek, E., Galliano, F., & Jones, A. P. 2007, ApJ, 662, 927
Fazio, G. G., Hora, J. L., Allen, L. E., et al. 2004, ApJS, 154, 10
Gal-Yam, A., Leonard, D. C., Fox, D. B., et al. 2007, ApJ, 656, 372
Granot, J., & van der Horst, A. J. 2014, PASA, 31, 8
Gruendl, R. A., Chu, Y.-H., Van Dyk, S. D., & Stockdale, C. J. 2002, AJ, 123, 2847
Houck, J., Roellig, T., van Cleve, J., et al. 2004, ApJS, 154, 18
Hurley-Walker, N., Callingham, J. R., Hancock, P. J., et al. 2017, MNRAS, 464, 1146
Jacobs, B. A., Rizzi, L., Tully, R. B., et al. 2009, AJ, 138, 332
Kiewe, M., Gal-Yam, A., Arcavi, I., et al. 2012, ApJ, 744, 10
Kotak, R., Meikle, W. P. S., Farrah, D., et al. 2009, ApJ, 704, 306
Kuncarayakti, H., Maeda, K., Anderson, J. P., et al. 2016, MNRAS, 458, 2063
Lakićević, M., van Loon, J. Th., Stanke, T., De Breuck, C., & Patat, F. 2012, A&A, 541, L1
Laporte, N., Ellis, R. S., Boone, F., et al. 2017, ApJL, 837, L21
Makovoz, D., & Marleau, F. R. 2005, PASP, 117, 1113
Matsuura, M., Dwek, E., Barlow, M. J., et al. 2015, ApJ, 800, 50
Matsuura, M., Dwek, E., Meixner, M., et al. 2011, Sci, 333, 1258
McMullin, J. P., Waters, B., Schiebel, D., et al. 2007, in ASP Conf. Ser. 376, Astronomical Data Analysis Software and Systems XVI, ed. R. A. Shaw, F. Hill, & D. J. Bell (San Francisco, CA: ASP), 127
Meikle, W. P. S., Kotak, R., Farrah, D., et al. 2011, ApJ, 732, 109
Meikle, W. P. S., Mattila, S., Pastorello, A., et al. 2007, ApJ, 665, 608
Meunier, C., Bauer, F. E., Dwarkadas, V. V., et al. 2013, MNRAS, 431, 2453
Montes, M. J., Weiler, K. W., & Panagia, N. 1997, ApJ, 488, 792
Nozawa, T., Kozasa, T., & Habe, A. 2006, ApJ, 648, 435
Pei, Y. C., Fall, S. M., & Bechtold, J. 1991, ApJ, 378, 6
Peters, W. L., Freeman, K. C., Forster, J. R., Manchester, R. N., & Ables, J. G. 1994, MNRAS, 269, 1025
Pettini, M., King, D. L., Smith, L. J., & Hunstead, R. W. 1997, ApJ, 478, 536
Qing, G., Wang, W., Liu, J.-F., & Yoachim, P. 2015, ApJ, 799, 19
Ryder, S., Staveley-Smith, L., Dopita, M., et al. 1993, ApJ, 416, 167
Ryder, S. D., Kotak, R., Smith, I. A., et al. 2016, A&A, 595, L9
Ryder, S. D., Staveley-Smith, L., Malin, D., & Walsh, W. 1995, AJ, 109, 1592
Sarangi, A., & Cherchneff, I. 2013, ApJ, 776, 107
Sault, R. J., Teuben, P. J., & Wright, M. C. H. 1995, in ASP Conf. Ser.77, Astronomical Data Analysis Software and Systems IV, ed. R. Shaw, H. E. Payne, & J. J. E. Hayes (San Francisco, CA: ASP), 433
Schlegel, E. M. 1990, MNRAS, 244, 269
Schlegel, E. M., Petre, R., Colbert, E. J. M., & Miller, S. 2000, AJ, 120, 2373
Schlegel, E. M., Ryder, S., Staveley-Smith, L., et al. 1999, AJ, 118, 2689
Smith, I. A., Ryder, S. D., Böttcher, M., et al. 2007a, ApJ, 669, 1130
Smith, N., Li, W., Filippenko, A. V., & Chornock, R. 2011, MNRAS, 412, 1522
Smith, N., Li, W., Foley, R. J., et al. 2007b, ApJ, 666, 1116
Szalai, T., Zsíros, S., Fox, O. D., Pejcha, O., & Müller, T. 2018, ApJ, submitted (arXiv:1803.02571)
Tanaka, M., Nozawa, T., Sakon, I., et al. 2012, ApJ, 749, 173
van Dyk, S. D. 2011, BAAS, 43, 21741003
Walker, M. A. 1998, MNRAS, 294, 307
Weiler, K. W., Panagia, N., & Sramek, R. A. 1990, ApJ, 364, 611
Weiler, K. W., Sramek, R. A., Panagia, N., van der Hulst, J. M., & Salvati, M. 1986, ApJ, 301, 790
Werner, M., Roellig, T., Low, F., et al. 2004, ApJS, 154, 1
Williams, B. F., Hillis, T. J., Murphy, J. W., et al. 2018, ApJ, 860, 39
Williams, B. J., Borkowski, K. J., Reynolds, S. P., et al. 2006, ApJL, 652, L33
Wilson, W. E., Ferris, R. H., Axtens, P., et al. 2011, MNRAS, 416, 832
Zhao, H.-H., Weng, S.-S., & Ng, C.-Y. 2017, MNRAS, 468, 1551